Article

A Comparison of Steam Turbine Control Valve Geometries and Their Dynamic Behavior at Part Load †

Christian Windemuth * , **Martin Lange** and **Ronald Mailach**

Chair of Turbomachinery and Flight Propulsion, Technische Universität Dresden, 01062 Dresden, Germany;
martin.lange@tu-dresden.de (M.L.); ronald.mailach@tu-dresden.de (R.M.)
* Correspondence: christian.windemuth@tu-dresden.de
† This paper is an extended version of our paper published in the Proceedings of the 15th European
Turbomachinery Conference, Budapest, Hungary, 24–28 April 2023.

Abstract: A growing significance of flexible steam turbine operation challenges the control of turbines, as part load operation using control valves can be accompanied by highly unsteady flow conditions. The increased dynamic load induced by pressure forces can reduce the reliable operating range, weaken the valve, and lead to mechanical failures. The geometry of the valve plays a major role in the reduction of dynamic forces. Using a scaled control valve, experiments were conducted with a focus on the dynamic behavior of the valve head. A spherical valve shape favoring unstable operation was used as a reference case, and the desired instability was proven by measurements. Different modified valve geometries based on literature featuring separation edges were then tested against the spherical shape. Results indicate the improved stability of the modified geometries over the reference geometry. For most of the operating range, vibrations were drastically reduced, and the overall flow stabilized.

Keywords: steam turbine; control valve; vibration; part load operation

1. Introduction

As a crucial component, steam turbines are involved in a major share of the electrical power conversion. With a steady increase of the contribution of volatile renewable energies, the compensation of grid imbalances becomes a major challenge, and part load operation a key demand for thermal power plants. Gas turbines provide high flexibility for on-demand regulation and the increasing demand of compensation power extends this requirements to the steam turbines of thermal power plants. In this context, the designed nominal load of future steam turbines is expected to shift from formerly base to part load. The current uncertainty of natural gas availability enhances this demand because the long term availability of gas fired units becomes less predictable.

Short-term regulation of steam turbines especially challenges the control unit, as the thermal inertia and large volume of the boiler limit large thermal gradients of the steam supply. As a solution, the use of control valves for fast load gradients is widely spread, while slow load gradients are compensated by sliding live steam pressure levels. According to Cziesla et al. [1], large scale power plants are usually operated at 95–98% loading. The remaining margin to maximum load provides on-demand power reserves by relieving the throttle valves to full openings, meeting the requirements for primary frequency control of electrical grids [2]. For reduced power demands, control valves can be further throttled into part load operation, usually followed by adjusting the live steam conditions. Within limitations by combustion stability and the thermal load of the boiler at very low flow rates, the combined measures enable typical part load operation of down to 40%, which can be extended to 25% for state-of-the-art hard coal fired units by a change of the boiler operation regime [3].

At throttled conditions, a significant amount of pressure energy is converted to kinetic energy as the flow passes the throttle area of the valve. Due to the following sudden increase

Int. J. Turbomach. Propuls. Power **2023**, *8*, 55

2 of 17

of the flow area, the flow is faced with a rapid pressure rise favoring flow detachments and vortex structures [4]. The resulting unsteady pressure fields yield in lateral and axial pressure forces acting on the valve support. In case of significant lateral displacements, the varying throttle area around the circumference can enhance the imbalance and asymmetric load. The support of the valve head needs to be sufficiently stiff to limit the magnitude of vibrations and resulting material stresses, especially if vibrations occur near mechanical frequencies of the structure. Literature data (e.g., [5]) and experiments confirm that natural frequencies are significantly excited by the flow.

The magnitude of vibrations is linked to the stability of the flow field, which in return is dependent of the geometric design and the operating point. As a simple valve design, spherical valve shapes have been implemented in a variety of turbines. The converging–diverging flow section provides a smooth transition as the flow passes the throttle area. Due to the Coandă Effect, the flow attempts to remain attached to the boundaries, resulting in a diverging flow path until the pressure rise triggers a separation of the flow. For the spherical geometry, an inevitable flow detachment occurs at smaller openings favorably at the valve seat due to its smaller radius. In this case, a flow impingement near the center is inevitable and results in local high pressure regions at the valve head.

Early investigations link the core flow to increased instability and noise, whereas an annular flow, separated from the head and attached to the seat and diffuser, was found to be more stable [6]. Attempts to stabilize the flow by geometric modifications often focused on these key flow patterns and force a flow detachment from the valve head by introducing a separation edge. Similar shapes can be found in more recent literature, especially with industrial backgrounds (e.g., [7–9]).

In recent decades, numerical methods became increasingly important and powerful, providing deeper insights into three-dimensional flows and allowing the numerical evaluation and optimization of geometries (e.g., [10]). At the same time, experimental data is rare and only available for limited cases. Numerical studies thus rely on limited fundamental validation data or case-specific studies. In the presented work, several valve shapes were investigated experimentally to enhance the availability of generic validation data. Because experiments were obtained from the same test rig, scale, and valve support, a unique comparison of fundamental valve shapes is provided and allows a direct comparison between geometries, which in return can be used for numerical validation by reported flow rates, pressure trends, and the dynamic load. For four generic valve modifications, flow rates for the whole operating range are presented and compared against the spherical reference shape. Pressure trends and frequency spectra as well as RMS values of lateral forces are additionally provided for a broad band of operating conditions.

2. Experimental Setup

Presented measurements were conducted with compressed air at the control valve test rig previously introduced in Windemuth et al. [11]. After selecting four different valve geometries, experiments were performed at constant opening ratios and increasing inlet pressures against the ambient back pressure. Time averaging measurements include a flow meter (RMG Turbine Meter TRZ 03, max. error $\pm 1\%$), pneumatic pressure sensors (max. error ± 40 Pa, p_{t0} ± 280 Pa), and temperature probes (max. error ± 0.5 K) used to calculate the flow characteristics. Additionally, time-resolving pressure transducers (*Kulite XCQ-080; 1.7 bar abs.; max. error $\pm 1\%$*) provide further insights into the time-dependent pressure field. For the presented analysis, the lateral forces acting on the valve head, recorded by strain sensor arrays *HBM 1-XY31-1.5/350* and *HBM 1-DY41-1.5/350* (full-bridge configuration), have been used to evaluate the operational stability. The noise level in the order of $1 \, \mathrm{N}/\sqrt{\mathrm{Hz}}$ for lateral forces and $30 \, \mathrm{N}/\sqrt{\mathrm{Hz}}$ for axial forces is considered the measure of uncertainty of force (strain) measurements, as it exceeds the raw accuracy of the data acquisition.

Int. J. Turbomach. Propuls. Power **2023**, *8*, 55

3 of 17

2.1. Reference Design

The shape of the control valve has a major influence on operational stability. During the design of the test rig, an unstable behavior was desired, and a spherical valve head (known to favor flow instability) was chosen in combination with a toric valve seat as shown in Figure 1 (dimensions provided in Table 1). The continuous valve head favors head-attached flows, resulting in impingements as the flow combines in the diffuser. More severe at smaller opening ratios, the corresponding flow instability triggers asymmetric pressure forces and can result in a significant dynamic loading of the support.

Table 1. Normalized valve geometry.

| Symbol	$[^1/_{D_S}]$	Description
D_S	1.00	Seat diameter
D_D	0.80	Diffuser throat diameter
H	OR	Valve lift H
		Opening ratio $OR = H/D_S$
R_P	0.72	Head radius
R_S	0.32	Seat (transition) radius
x_{PS}	0.23	Pressure sensor position
α	4.00°	Diffuser opening angle
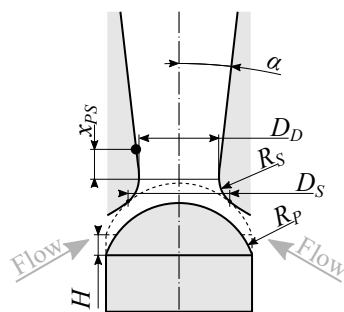
Figure 1. Geometry of the test valve.

With the aim to assess geometric modifications and their impact on operational stability, the spherical valve geometry is therefore used as the benchmark for the presented work.

2.2. Modified Geometries

With increasing pressure and temperature levels and power outputs, the stress of steam turbine components has continuously increased. As a result, reliable operation arose as a major challenge because flow-induced vibrations can significantly reduce component lifetimes and enhance the danger of mechanical failures and resulting outages [12].

At part load operation, large pressure gradients generate unavoidable high kinetic energies of which a large share is dissipated through turbulent structures. Great effort was therefore conducted to stabilize the overall flow by geometric modifications, aiming to reduce the asymmetry of unsteady pressure fields.

Among several strategies, a separation edge on the valve head proved itself as an effective measure to prevent near-head impingements and favor the more stable annular flow pattern. Variations of a backward facing step are therefore found in modern valve designs.

In the presented study, a side-by-side comparison of different generic geometries is presented with the selected valve shapes summarized in Figure 2.

The first three modifications in Figure 2 can be machined from existing spherical valve heads with an increasing share of removed material and obtuse (145°), right (90°), and acute (53°) separation edge angles. Motivated by results obtained from the tree modifications, the

Int. J. Turbomach. Propuls. Power **2023**, 8, 55

4 of 17

fourth *Concave* geometry (Figure 2d) was derived from idealized flow path assumptions and targeted an improved flow rate at large opening ratios.

All geometries are axisymmetric with the same characteristic seat diameter D_S, defined as the contact circle at closed conditions. As a direct cause, the absolute and normalized scale of all modifications was kept constant.


(**a**) Cutoff   (**b**) Backstep   (**c**) Can-like   (**d**) Concave
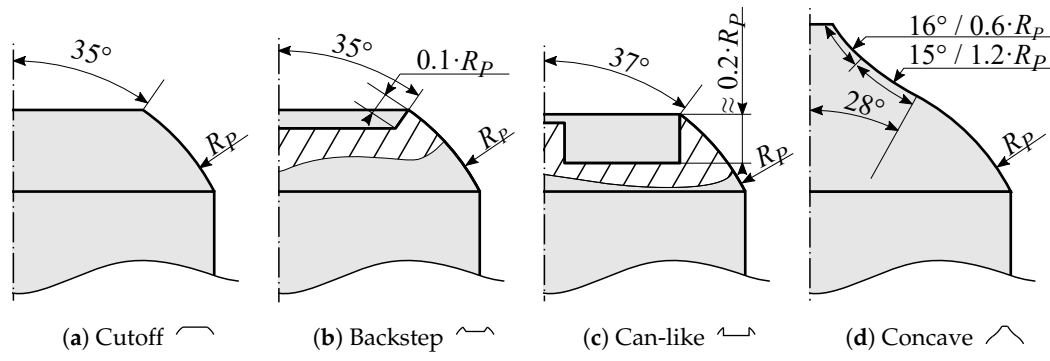
Figure 2. Modified valve geometries.

3. Results

3.1. Flow Characteristics

Consistent with the literature, the operating point of the valve is defined by the *opening ratio (OR)*, representing the absolute valve lift H normalized by the reference diameter D_S, and the *pressure ratio* ($PR = p_{amb}/p_{t0}$), defined by the ratio of the outlet static pressure, here specifically the ambient pressure p_{amb} in the test facility, to the inlet total pressure p_{t0}. At the test rig, arbitrary combinations of PR and OR can be investigated, and for all geometries flow characteristics were derived, provided in Figure 3.

The presented flow characteristics were recorded at constant opening ratios and variable (increasing) inlet pressures against the constant (ambient) back pressure and are provided as reduced flow rates $q(OR, PR)$, defined as

$$q = \frac{\dot{m} \cdot \sqrt{T_{t0}}}{p_{t0} \cdot A_D \cdot q^*} \, . \tag{1}$$

Normalized by q^*, the theoretical maximum for $Ma = 1$ (assuming constant specific heat and ideal gas behavior) calculated as

$$q^* = \sqrt{\frac{\kappa}{R}} \cdot \left[1 + \frac{\kappa - 1}{2} \right]^{\frac{1}{2} \cdot \frac{1+\kappa}{1-\kappa}}, \tag{2}$$

values of q can range from 0 to 1. For the presented trends, a correction for pressure driven deformations proportional to the inlet gauge pressure in the form of $\Delta H \sim (p_{t0} - p_{amb})$ was applied, as the pressure load causes a deformation of the valve chest in the magnitude of tenth of μm.

In all sub-figures, solid lines compare the flow rate of the modified geometries against the spherical shape (dashed lines). For better visibility, regions of significant deviations against the reference case are highlighted in red (reduction) or green (increase).

Unlike experimental conditions, field operation is typically constrained to an operating line by the downstream turbine. The diagonal solid line represents such an operating line, along with the grey area indicating the expected range of possible operating lines, both assuming choked inlet conditions at the fictive downstream turbine. Operating lines with a steeper slope result in higher pressure losses at full load but allow smaller valves for the same (absolute) flow rate. The acceptable pressure loss of (geometrically) open valves at the design point is estimated to be in the order of 1 % (solid line), and the bounds of the shaded area represent full load pressure losses of 2 % to 0.5 % (values also apply to other figures).

Int. J. Turbomach. Propuls. Power **2023**, *8*, 55

5 of 17

For increasing opening ratios, the maximum normalized flow rates in Figure 3 approach the ideal value of 1. Even though, for openings above $OR \approx 0.23$, the valve is geometrically fully opened, the effective flow path is slightly reduced by boundary layers and detachments, resulting in a further increase as the valve is opened beyond the point at which $OR = 0.5$.
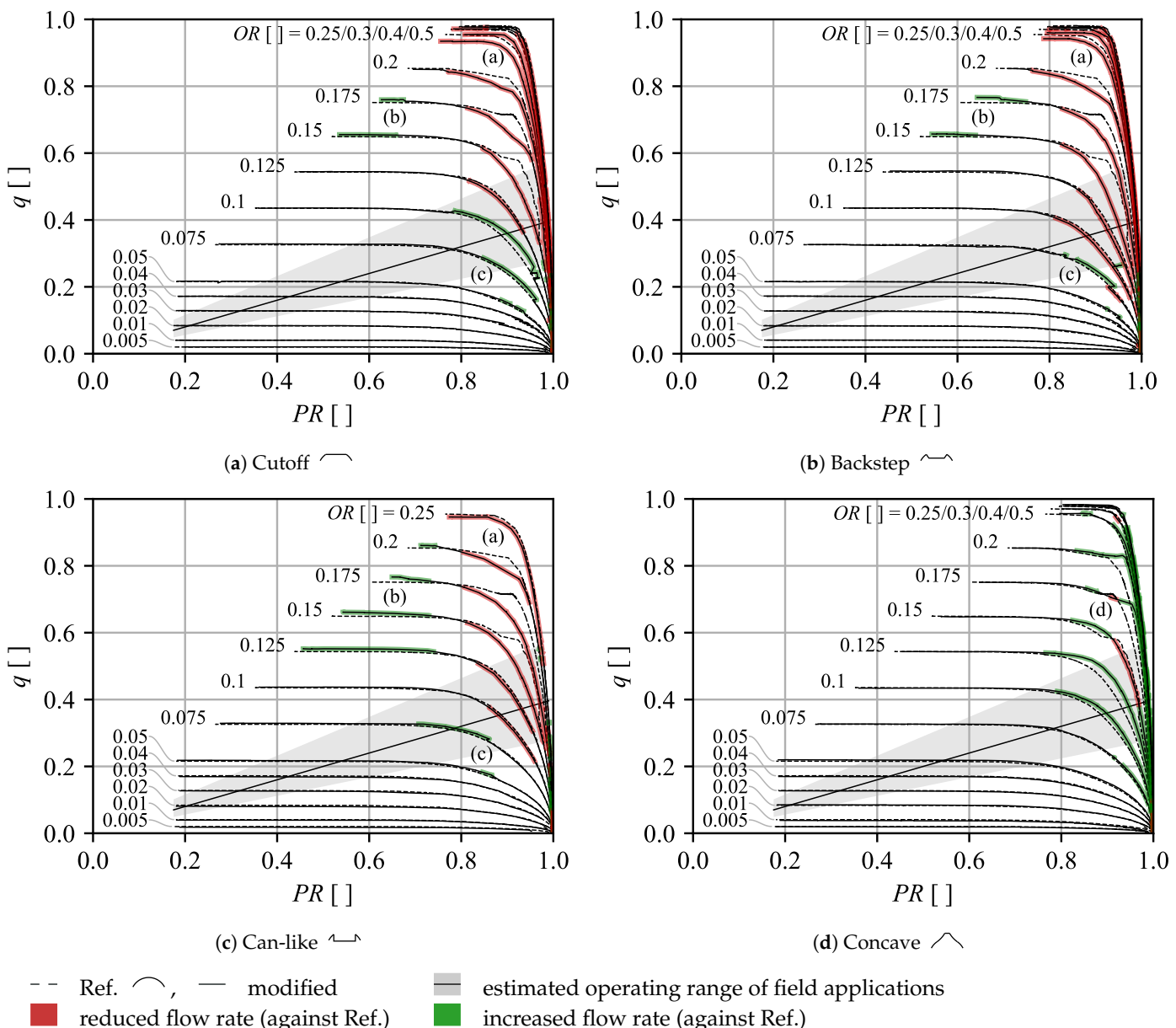

Figure 3. Flow characteristics of the modified valves and deviation to the spherical reference design.

Comparing the effect of the modifications with separation edges in Figure 3a–c, a significant reduction in the flow rate is observed in region (a) at large opening and pressure ratios. At large pressure ratios, this region partly extends into the estimated operating range. It is expected that this reduction is a direct result of the desired flow separation, further discussed in Figure 4.

As visualized for the spherical and *Backstep* geometry in Figure 4a, the position of the smallest flow section of the three-dimensional (3D) geometry does not align with the tightest gap between valve head and seat (2D). As the flow passes the gap, the downstream flow section is further reduced as the radial distance to the valves center line decreases, even though the cross section suggests a diverging flow path. For larger valve openings,

Int. J. Turbomach. Propuls. Power **2023**, *8*, 55

6 of 17

this effect is enhanced; as a result, the actual throttle area for the reference design moves past the location of the separation edge, as sketched for the *Backstep* geometry (left side of Figure 4a). Assuming that the flow direction remains unchanged during separation, the introduction of the separation edge therefore reduces the effective valve throat in comparison to the spherical shape and results in significantly reduced flow rates previously observed in region (a) in Figure 3a–c. Based on this finding, the *Concave* geometry was designed to maintain or improve the initial flow rate by reshaping the valve head to follow the boundary of the assumed recirculation area of the spherical valve (dashed blue line in Figure 4a). The result is clearly visible in region (d) in Figure 3d and shows that subsonic flow rates are in part significantly increased compared to the reference (and other) geometries, while maximum (choked) flow rates are maintained.


(**a**)   (**b**)
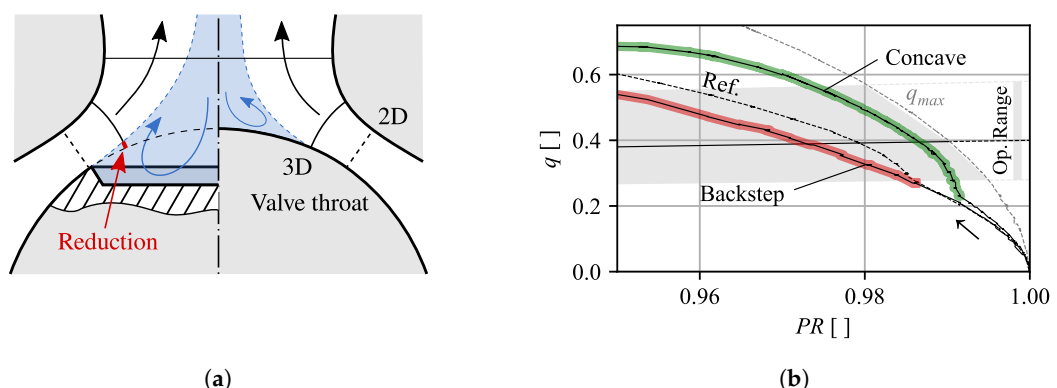
Figure 4. Impact of forced detachments on flow rates at large valve openings and a snippet of $OR = 0.175$ from region (a) in Figure 3b/region (d) in Figure 3d. (**a**) Reduced effective valve throat by detached subsonic flows. (**b**) Detailed view of flow rates at $OR = 0.175$ for Backstep and Concave geometries.

Figure 4b demonstrates the increase more clearly by a detailed view of $OR = 0.175$ for the *Backstep* and *Concave* geometries. In the range of $PR \approx 0.96$ to 0.98, the flow rate is increased by roughly 50 % compared to the *Backstep* and even 20–30% compared to the spherical shape, indicating a delayed detachment from the valve head.

To a smaller extent, the improved flow rate can also be observed for smaller and larger opening ratios, even for geometric openings at above 100% (Figure 3d). While a reduced flow rate at throttled conditions can be compensated by a larger valve opening (constrained by the operating line), the reduced flow rate by the separation edge at maximum opening can possibly not be compensated. Based on the measurements, the *Concave* geometry is expected to provide reduced full load pressure losses compared to the spherical shape, while a slight increase is expected for the other modifications.

Also linked to the separation edge, an inverse behavior is observed in region (b) in Figure 3a–c. At supersonic flow conditions below $PR = 0.7$, an under-expanded flow condition is expected at the separation edge, resulting in an expansion of the flow into the former recirculation zone. In contrast to the reduced flow section discussed in Figure 4a, the expansion is expected to increase the effective throat and thus slightly increasing the flow rate. Because this region is far outside the expected range of field applications, it is not further discussed within this paper.

3.2. The Occurrence of Annular Flow Regimes at Throttled Valve Operation

In Figure 3a–c, a third region (c) is characterized by a spontaneous increase of the flow rate for opening ratios of 0.05 to 0.1 in the range of the expected part load operation. For better visibility, a detailed view of the flow rate at $OR = 0.075$ is provided in Figure 5 for the *Cutoff* geometry along with pneumatic wall pressure trends (sensor position in Figure 5c,d).

Int. J. Turbomach. Propuls. Power **2023**, *8*, 55

7 of 17
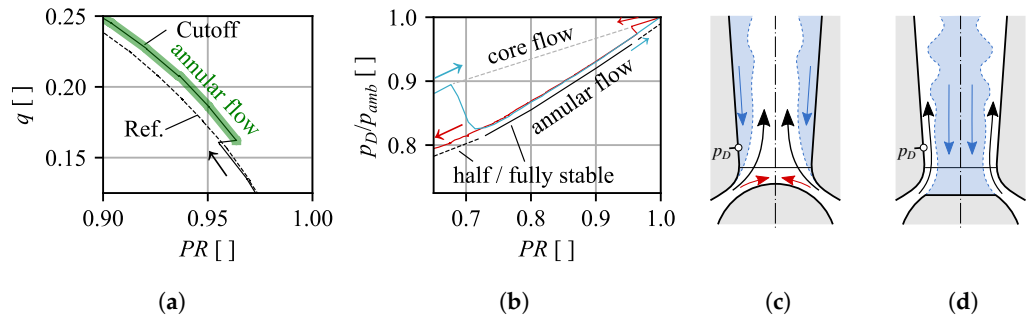
Figure 5. Exemplary detail of the spontaneous change between annular and core flow regimes at *OR* = 0.075 for the Cutoff geometry (detailed view of region (c) in Figures 3a and 6b). (**a**) Normalized flow rate. (**b**) Wall pressure trend. (**c**) Core flow. (**d**) Annular flow.
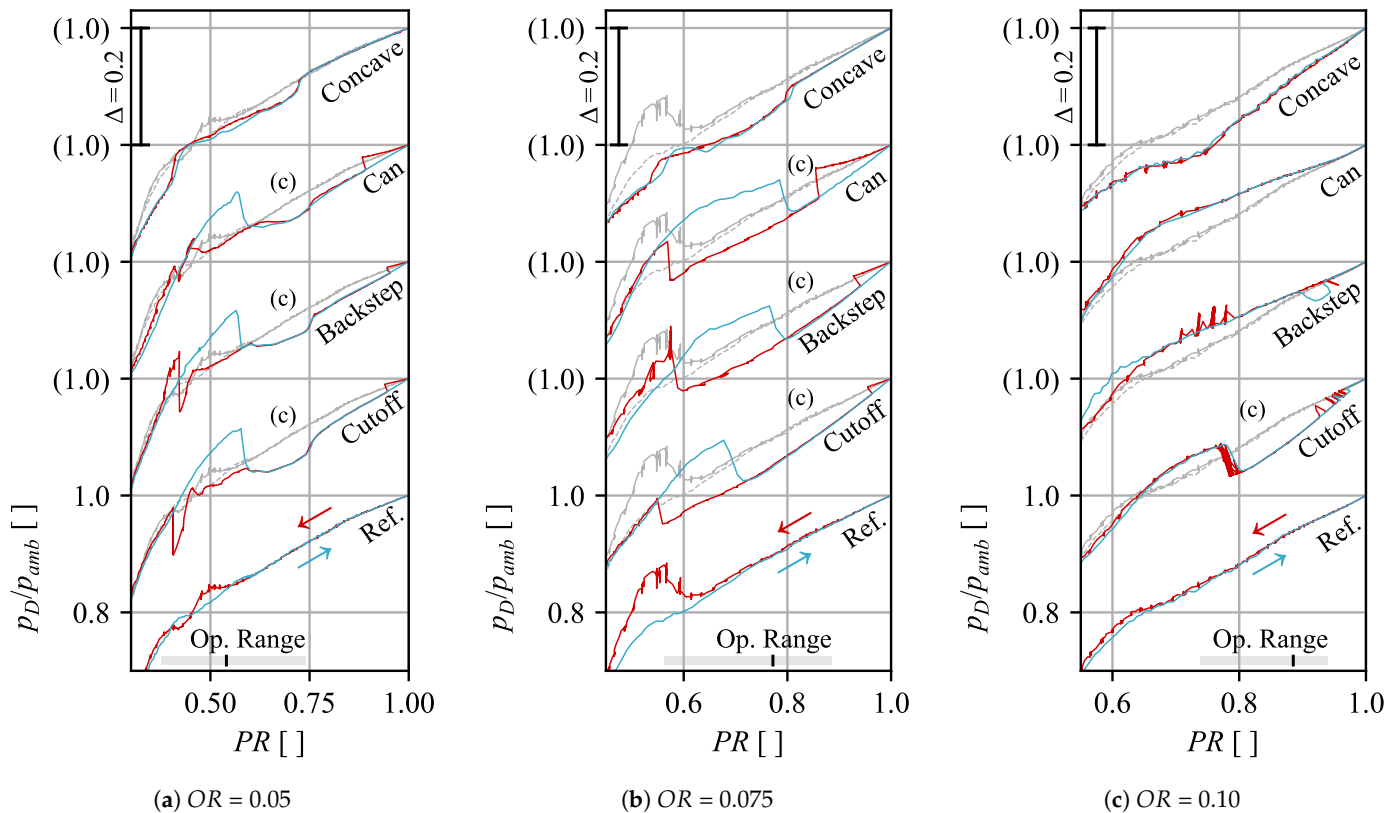

Figure 6. Wall pressure trends at the diffuser inlet for the investigated geometries.

As the pressure ratio in Figure 5a is reduced and approaches $PR = 0.95$, a sudden jump onto a separate (higher) flow characteristic is observed. Simultaneously, the corresponding pneumatic pressure measurement (the red curve in Figure 5b) shows a significant drop in the wall pressure.

In Figure 5b (and later Figure 6), the red curves were recorded at decreasing PR and correspond to the flow characteristics. Due to the settling time of the flow and temperature measurements, and to prevent transients within time-resolving pressure measurements, these measurements include hold times (as partly visible in the red unfiltered pressure trends in Figure 6). The blue curves in turn were derived after the actual measurements during the de-pressurization of the test rig (increasing PR) at continuous and faster pressure gradients. While flow measurements during the de-pressurization become invalid due to a lag, pressure measurements respond quicker and allow an additional comparison in the reverse direction. Because the de-pressurization was limited by maximum pressure gradients of instrumentation, a quasi-steady state with respect to the valve's operating point is still assumed due to the high velocities, despite the faster rate.

Int. J. Turbomach. Propuls. Power **2023**, *8*, 55

8 of 17

Consistent with the flow rate, the actual measurement (red, decreasing *PR*) and the de-pressurization of the test rig (blue, increasing *PR*) clearly follow two distinct pressure branches, suggesting two different and temporal stable flow regimes. Based on measurements and supported by CFD, the lower branch can be linked to the desired annular flow (Figure 5d). At this time, the investigated wall pressure sensor is exposed to a high velocity flow adjacent to the diffuser wall, which results in low pressure readings. The upper branch on the other hand corresponds to detached flow conditions (Figure 5c), where the sensor is exposed to the higher pressure inside the recirculation zone.

The same behavior was also found for the *Backstep* and *Can-like* geometries as shown in Figure 6 for opening ratios of 0.05, 0.075, and 0.1. In all three cases with separation edges (curves are vertically shifted by an offset of 0.2), the two distinct flow regimes are observed for $OR = 0.05$ and 0.075 with different extents. At $OR = 0.1$, only the *Cutoff* and *Backstep* shape were able to trigger the annular flow, which only for the first geometry is stable over a wider range.

For all three modifications with a separation edge, a region of the annular flow regime, which is independent of the direction of pressure change, can be identified. Where applicable, it is marked with (c) in Figure 6 and corresponds to the range marked with a black solid line and labeled *fully stable* in Figure 5b (*Cutoff*, $OR = 0.075$).In case of the obtuse edge (*Cutoff*), this range is significantly stretched compared to the sharp-edged *Can-like* geometry. In most cases, the range of the stable annular flow pattern is bounded by two hysteresis regions at both ends (labeled *half stable* and marked by the dashed black line in Figure 5b). The right hysteresis loop extends up to $PR = 1$ and suggests that, once the annular flow is triggered, it is retained as long as fluid is passing the valve. The left loop on the other hand is bounded by a pressure jump towards the core flow regime (visible in Figure 6) and is expected to be triggered once the pressure gradient, which ties the flow to the wall, is not able to keep up with the increasing momentum of the inflow. Due to the hysteresis, the previous flow state is maintained for both core and annular flows across the *half stable* region. Except for the hysteresis bounds, both flow regimes are stable in itself (no switching, exception at $OR = 0.1$ in Figure 6c). As shown in Figure 6, the range in which both stable and half stable annular flows are observed, aligns with the estimated operating range (bottom). Similar flow conditions are therefore expected for field applications at part load conditions.

In contrast to the two distinct pressure branches, both the spherical and *Concave* geometry generally follow the same trends in both directions. The spherical valve shape (copy provided in grey) lies mostly between the core and annular flow branches. It is expected that the spherical valve is accompanied by a reduced symmetry of the flow and a possible oscillation between a locally attached and detached flow around the circumference along with locally reduced or increased flow rates. Because the time-averaging measurements (flow meter and pneumatic pressure sensors) cannot capture these time-variant conditions, results in Figures 3 and 6 are expected to represent a blend of the two states. Because both flow patterns are expected to exist and propagate along the circumference, the smoother transitions and the lack of a hysteresis can be explained as the fraction of either of the two flow state's increases or decreases. Slightly lower pressure levels have been recorded for the *Concave* shape, possibly caused as the flow is guided towards an axial flow direction resulting in increased flow velocity near the wall with respect to reduced pressure levels.

Concluding from the observations, it is expected that pure annular and axisymmetric flow regimes in the discussed operating range only exist for the geometries with distinct separation edges on the valve head.

3.3. Flow-Induced Pressure Forces

The time-averaged static pressure trends discussed above indicated that introducing a separation edge successfully triggered desired annular flows within the expected part load operating range, suggesting increased operational stability. In the conducted experiments, time-resolving pressure and strain measurements were used to draw a respective conclusion

Int. J. Turbomach. Propuls. Power **2023**, *8*, 55

9 of 17

on flow stability and unsteady dynamic load, which will be exemplary discussed by comparing the *Backstep* geometry to the spherical reference case at $OR = 0.075$ in Figure 7. Through a side-by-side comparison of wall pressure trends (top), its corresponding power spectral density (middle), and the RMS level of lateral forces (bottom), the impact of the modification with regions of a pure annular flow is presented. The presented data were recorded during pressurization of the valve chest (decreasing PR), corresponding to the red curves in Figure 6.
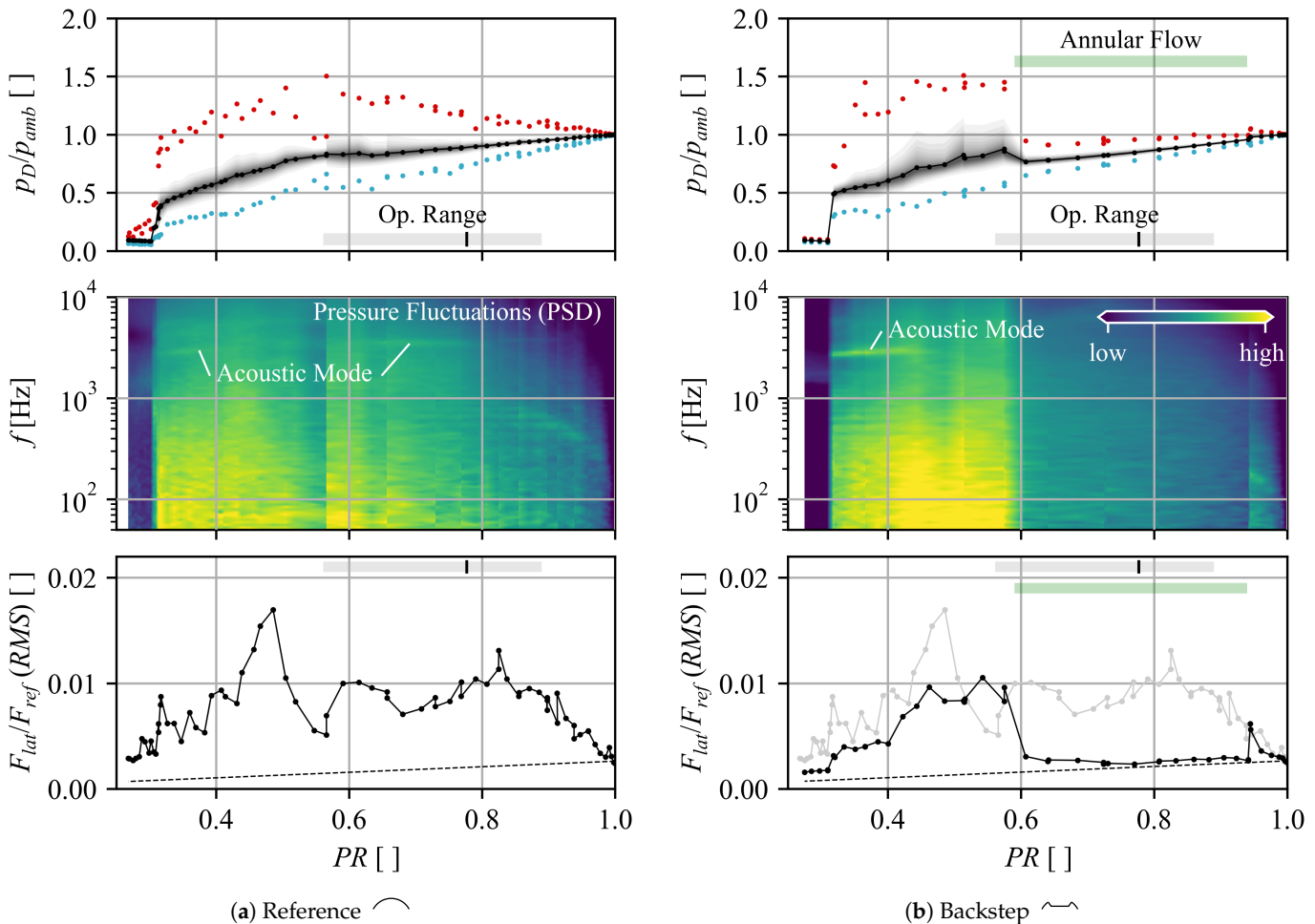

Figure 7. Influence of the geometric modification and annular flow on the wall pressure and dynamic load at $OR = 0.075$.

For both geometries, the wall pressure trends at the diffuser inlet are provided in the first row of Figure 7 (the same axial position as previously discussed pneumatic sensor), including average (black), minimum (blue), and maximum (red) readings from time-resolving measurements. The shaded patches represent quantiles from 2.5–97.5% at 2.5% steps, providing additional information on the scattering of pressure readings.

For the presented *Backstep* modification in Figure 7b, the previously discussed pressure drop indicating the annular flow regime is also visible in time-resolving measurements from $PR \approx 0.94$ to 0.58 (green bar, labeled *Annular Flow*). Within this range, both average pressure fluctuations as well as pressure spikes are significantly reduced, visualized by the quantiles, minimum, and maximum readings. Below this region from $PR = 0.58$ to 0.3, the influence of the geometric modification fades, and amplitudes are of similar magnitude or even increased in comparison against the spherical shape as visible by the quantile patches and maximum values.

For high flow rates (low pressure ratios), a rapid drop of the pressure level and pressure amplitudes can be observed independently of the valve shape (at $PR \approx 0.3$

Int. J. Turbomach. Propuls. Power **2023**, *8*, 55

10 of 17

for $OR = 0.075$). At this point, a normal shock evolves and an attached axisymmetric supersonic flow is observed at the sensor's position. Simultaneously, wall pressures drop and become almost steady, eliminating most of the unsteady pressure forces acting on the valve support. Because the occurrence is far outside the expected operating range, this range is not further discussed, as it is expected to be irrelevant with respect to field applications (refer to Windemuth et al. [13] for further details).

The power spectral density (PSD) of the same pressure signals is shown in the second row in Figure 7 for 1/12th-octave bands, indicating a continuous increase of low frequency broad band amplitudes as the pressure ratio is decreased for the reference design. In this low frequency region, large vortex structures as discussed in Windemuth et al. [13] are observed in CFD results, showing slow and random propagations. The modified *Backstep* geometry shows a similar distribution of amplitudes outside the range of the annular flow. Within the range of the annular flow, a drastic reduction in amplitudes is captured across all frequency bands, spontaneously increasing back towards the reference level once the flow detaches again.

While most amplitudes in the power spectral density are concentrated in the form of random noise at lower frequencies, few distinct frequencies can be identified for both geometries. At around $PR = 0.3$ to 0.5, the first lateral acoustic mode near 3000 Hz is clearly excited. In comparison to the spherical shape, the acoustic mode can be identified much sharper for the *Backstep* shape, which is also observed for the other modifications. It is expected that, in case of the spherical shape, the increased asymmetry of the flow dampens periodic excitations, while the increased symmetry of the flow for modified geometries favors these structures.

In the bottom part of Figure 7, the dynamic load of the valve support is presented as the RMS level of the combined lateral force, normalized by a reference force $F_{ref} = p_{t0} \cdot A_{ref}$ derived from the area $A_{ref} = \pi/4 \cdot D_S^2$ and the inlet total pressure.

Consistent with the pressure trends, the magnitude of lateral forces mirrors the occurrence of pressure fluctuations, peaking at $PR \approx 0.48$ for the reference case. By introducing the separation edge and favoring the annular flow, the loading of the valve support is reduced by more than 50 %, shrinking RMS levels towards the noise floor of the strain measurements (dashed line). Even outside of the annular region and despite a small range at $PR = 0.55$, resulting forces are either maintained or reduced by the modification. For further information and extending Windemuth et al. [14], results from all geometries at opening ratios 0.05, 0.075, and 0.1 are provided in Appendix A in Figures A1–A5. While a similar behavior is observed for the other geometries comprising a separation edge, the *Concave* geometry shows less clear trends in terms of operation stability, even though the flow is guided towards an axial core flow. Nevertheless, pressure trends indicate increased flow stability and reduced forces at lower opening ratios.

4. Conclusions

In the presented study, an experimental side-by-side comparison of different valve geometries was provided and proved a strong impact of the valve shape on flow characteristics and flow stability.

The introduction of a separation edge was confirmed to trigger an annular flow at opening ratios of $OR \leq 0.1$, resulting in a significant reduction in wall pressure fluctuations and the dynamic component of lateral forces at expected part load conditions. Among the geometries with a forced separation, the extent of the improved operating range was found to be largest for the obtuse separation edge (*Cutoff*) and decreased with more acute angles (*Backstep* and *Can-like*). In most cases, the operating range of observed annular flows is bounded by hysteresis regions as the flow pattern changes from the attached to the detached state and vice versa.

Besides the improved flow stability, the annular flow at smaller valve openings showed increased flow rates compared to the spherical valve design, while flow rates at large openings were significantly reduced. The deviation of flow rates at small openings can be

Int. J. Turbomach. Propuls. Power **2023**, *8*, 55

11 of 17

compensated by adjusting the valve lift and is expected to be less crucial as the valve is constrained to the operating line. Observed sudden changes of the normalized flow rate, on the other hand, are considered potentially harmful, as the rapid increase or decrease of the pressure gradient across the valve affects components within, upstream, and downstream of the valve. Increased pressure losses at large (and full) valve openings, observed for all geometries with separation edges even above $OR = 0.25$, possibly cannot be compensated and may result in reduced full load efficiency.

Based on previous observations, the *Concave* valve head was successfully designed to encounter the increased full load pressure losses, providing the smallest pressure loss among all geometries across a wide range of valve openings. Around estimated full load operation, the *Concave* geometry was able to reduce the pressure loss, potentially improving overall efficiencies. In terms of pressure fluctuations and flow stability, the *Concave* geometry performed comparably to the spherical reference with significant improvements only visible at small opening ratios.

Based on the presented results, further experiments will be conducted with a reduced valve stiffness, and parallel CFD studies will be used to enhance the understanding of the three-dimensional flow. Based on all results, further geometric modifications will be considered for a further stabilization of the flow at part load operation.

Institutional Review Board Statement: Not applicable.

Informed Consent Statement: Not applicable.

Data Availability Statement: Data is contained within the article.

Abbreviations

The following abbreviations are used in this manuscript:

	Abbreviations	PR	pressure ratio: p_{amb}/p_{t0}
CFD	Computational Fluid Dynamics	p	pressure
PSD	Power Spectral Density	q	normalized flow rate
RMS	Root Mean Square	q^*	q at $Ma = 1$
		R	radius; specific gas constant
	Variables	T	temperature
α	diffuser opening angle	x	axial distance to diffuser throat
κ	isentropic exponent		
A	area		**Subscripts**
D	diameter	0	inlet (valve chest)
E	Energy	amb	ambient/outlet
e	specific energy	D	diffuser
F	Force	kin	kinetic energy
f	frequency	P	head (plug)
H	valve lift	PS	pressure sensor (position)
Ma	Mach Number	ref	reference
$\dot{m}$	mass flow	S	seat (radius, contact circle)
OR	opening ratio: H/D_S	t	stagnation/total

Int. J. Turbomach. Propuls. Power **2023**, *8*, 55

12 of 17

Appendix A
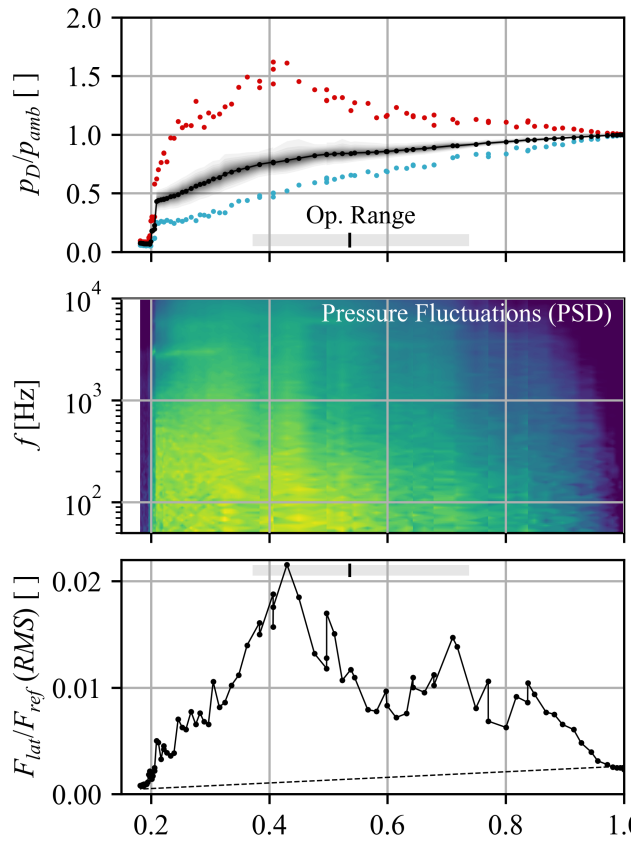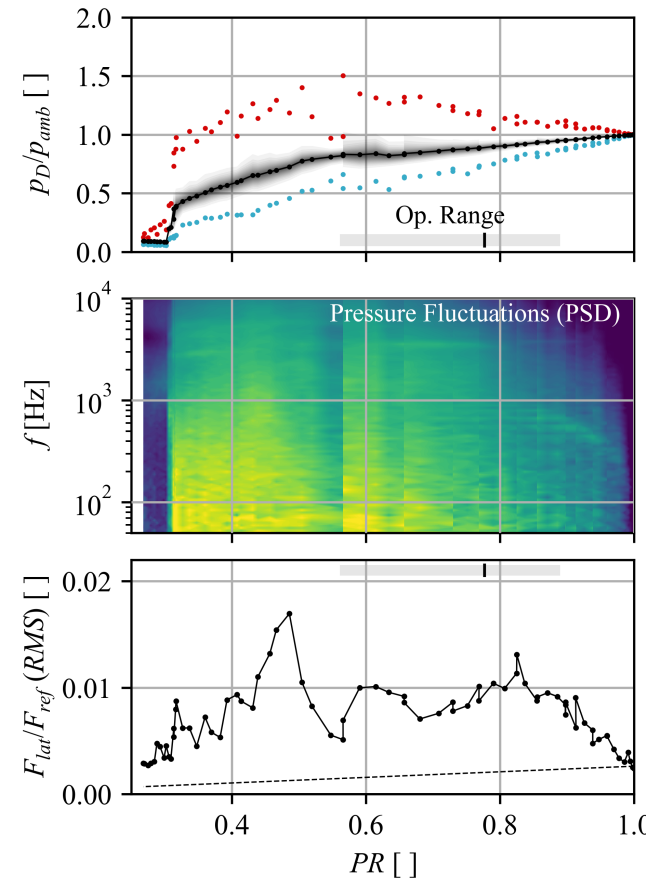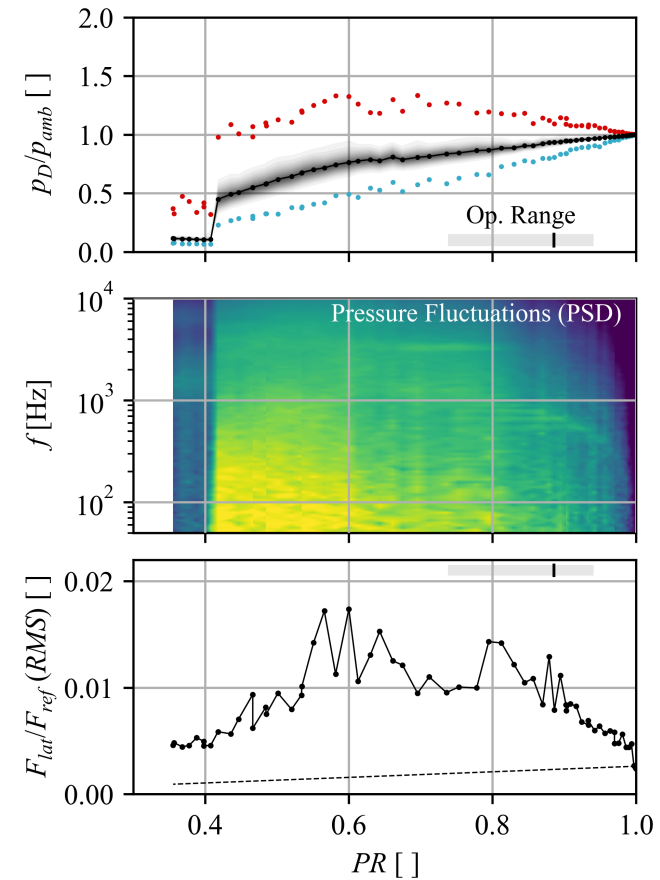
(**a**) $OR = 0.05$ (**b**) $OR = 0.075$ (**c**) $OR = 0.10$

Figure A1. Wall pressure trends, frequency spectra, and dynamic load for the Reference case.

Int. J. Turbomach. Propuls. Power **2023**, *8*, 55

13 of 17

Figure A2. Wall pressure trends, frequency spectra, and dynamic load for the Cutoff geometry.

Int. J. Turbomach. Propuls. Power **2023**, *8*, 55

14 of 17
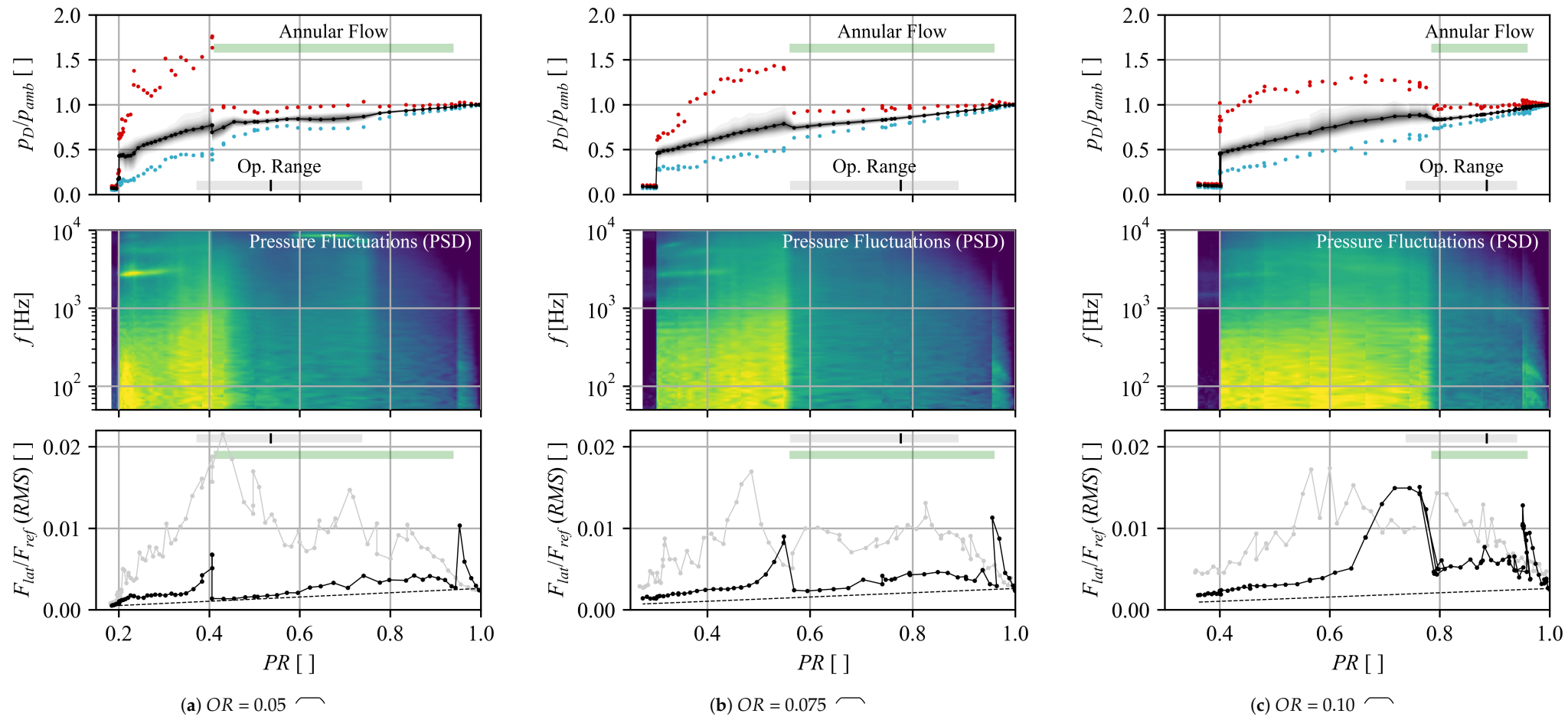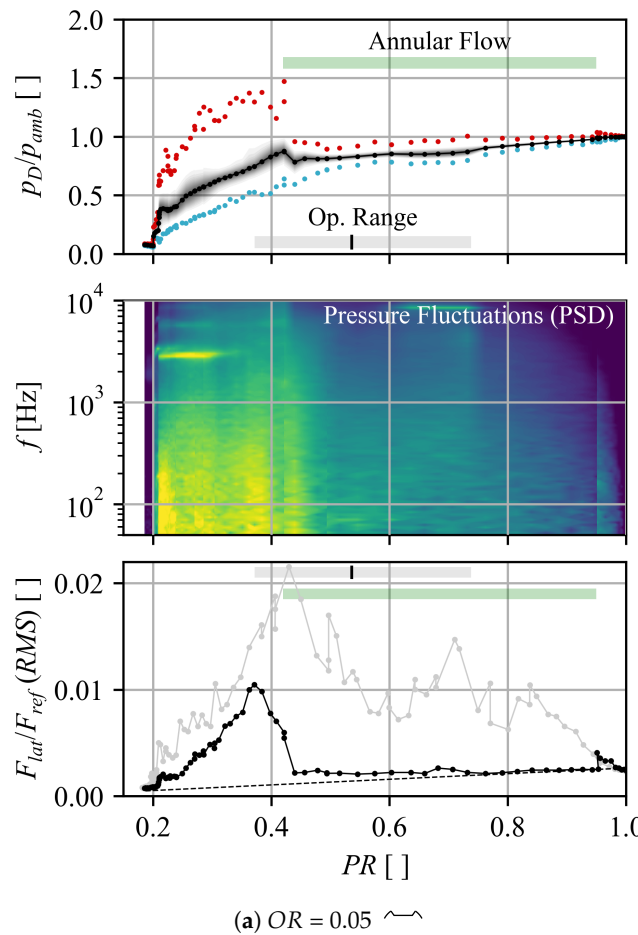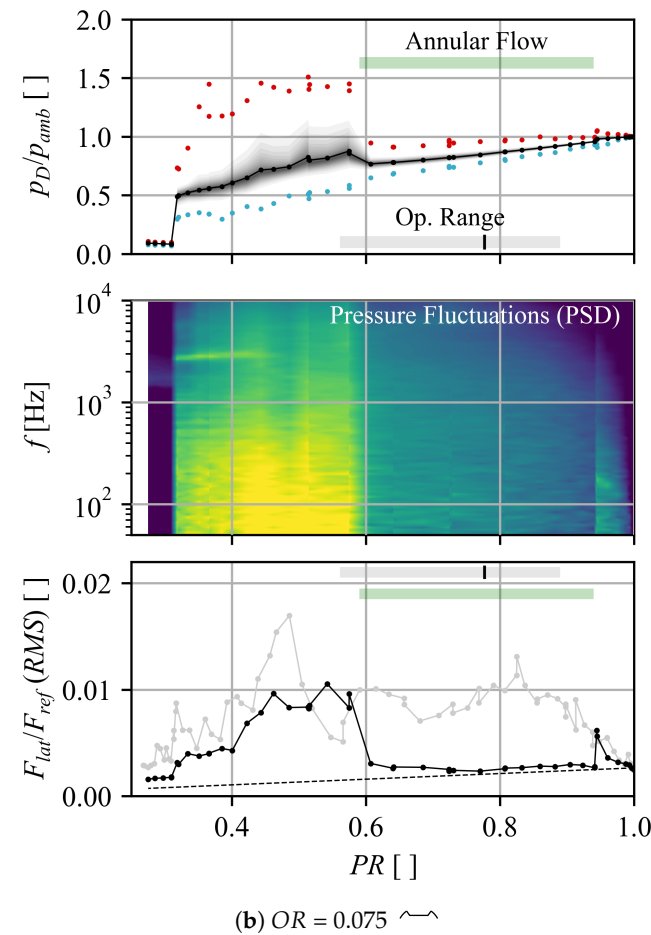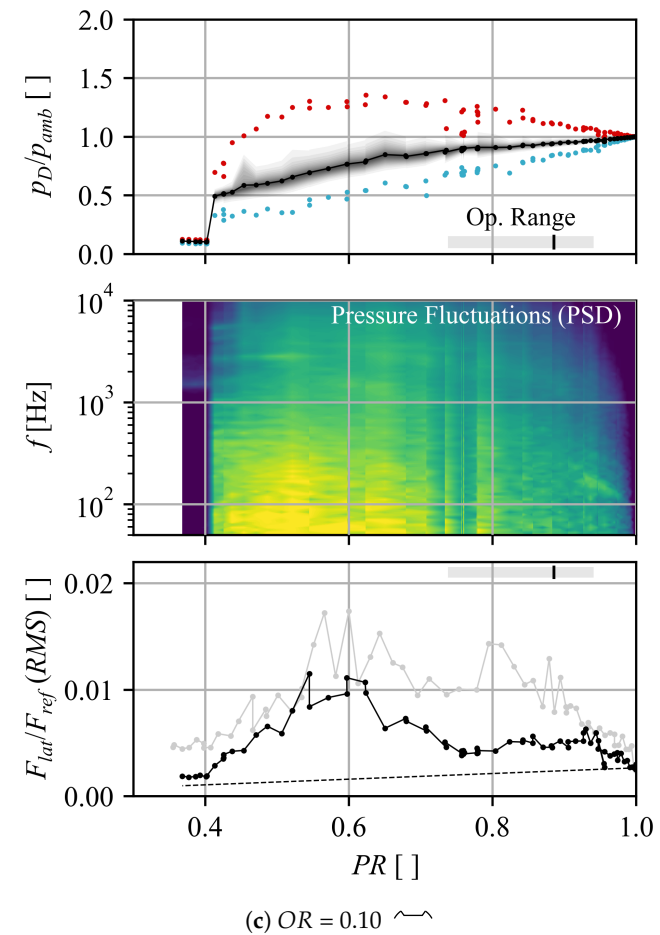
Figure A3. Wall pressure trends, frequency spectra, and dynamic load for the Backstep geometry.

Int. J. Turbomach. Propuls. Power **2023**, *8*, 55

15 of 17
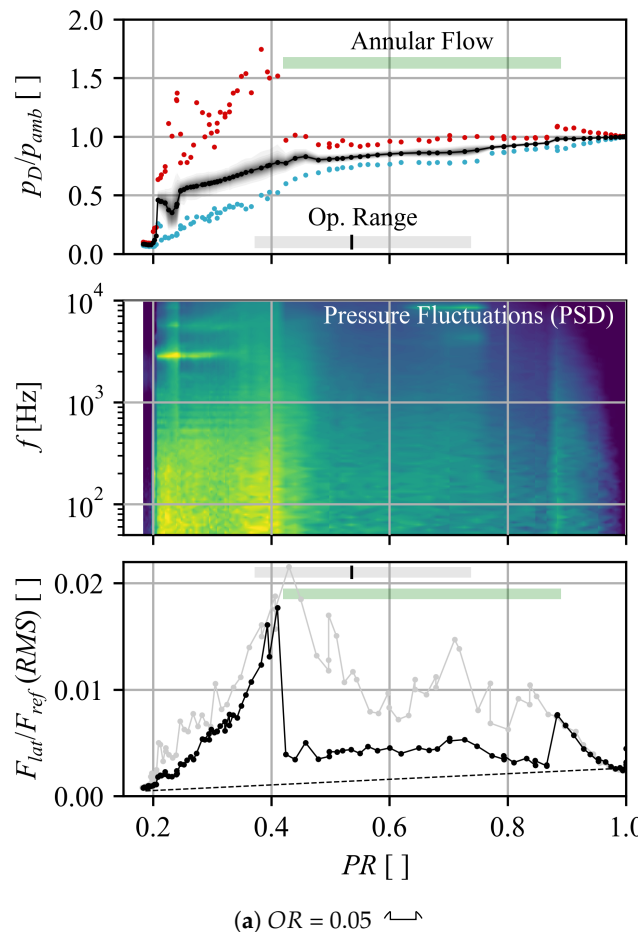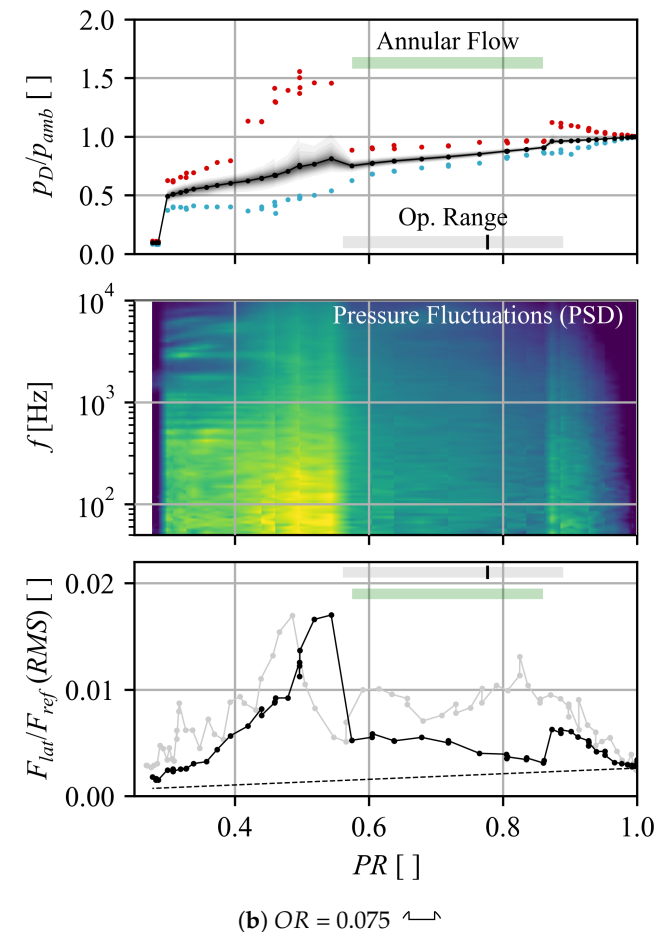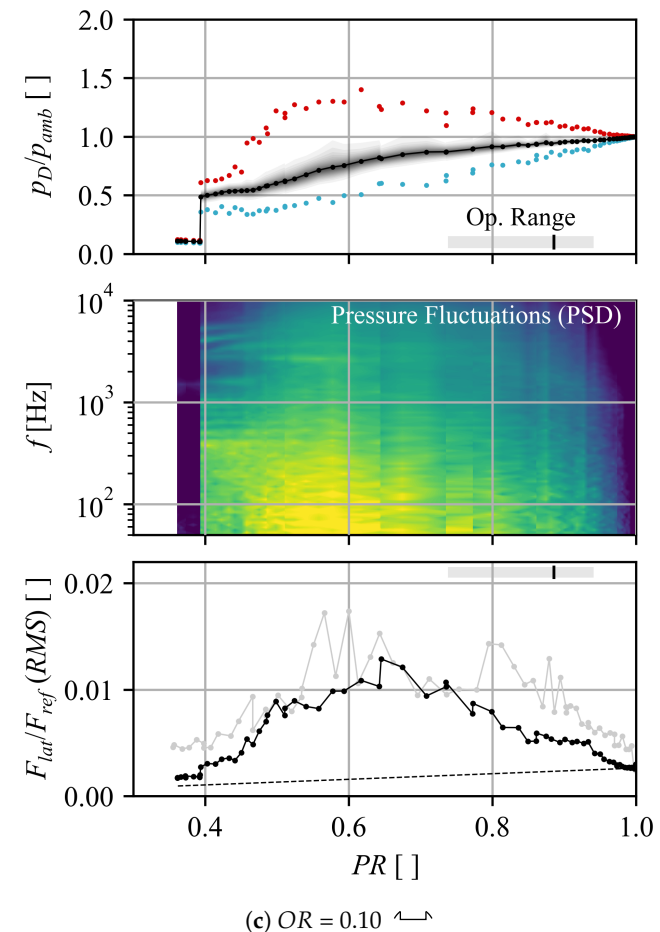
Figure A4. Wall pressure trends, frequency spectra, and dynamic load for the Can-like geometry.

Int. J. Turbomach. Propuls. Power **2023**, *8*, 55

16 of 17
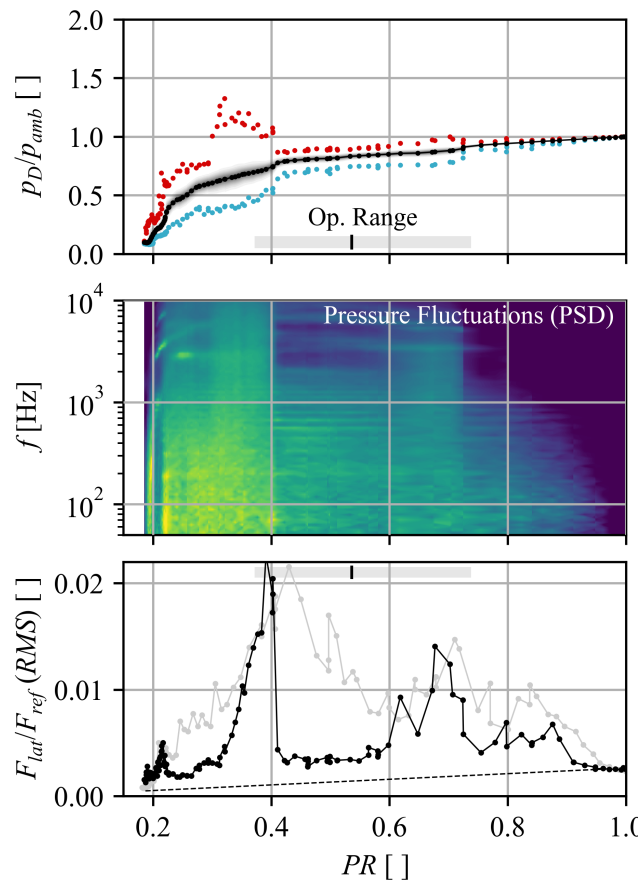
(a) *OR* = 0.05 ⌒
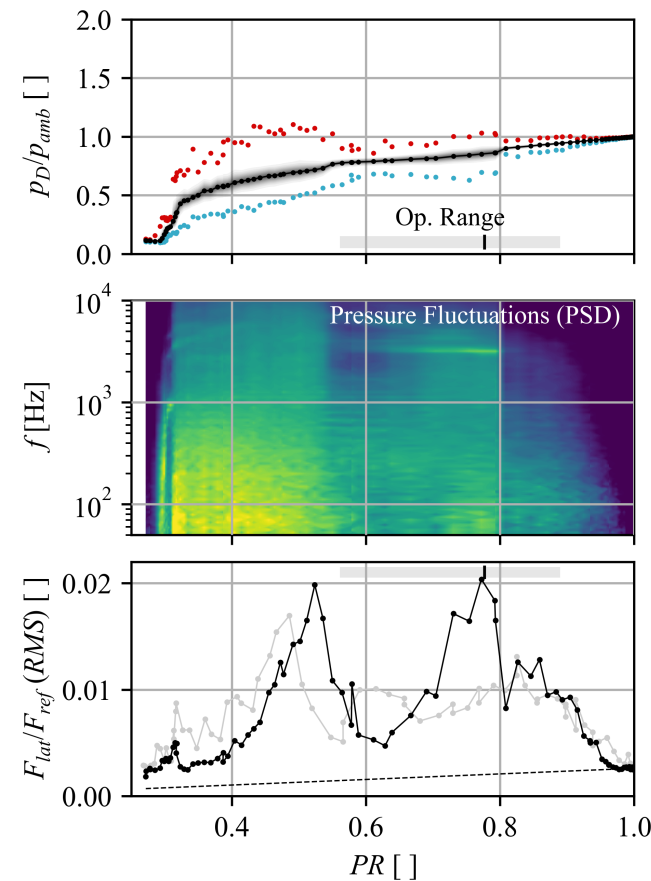
(b) *OR* = 0.075 ⌒
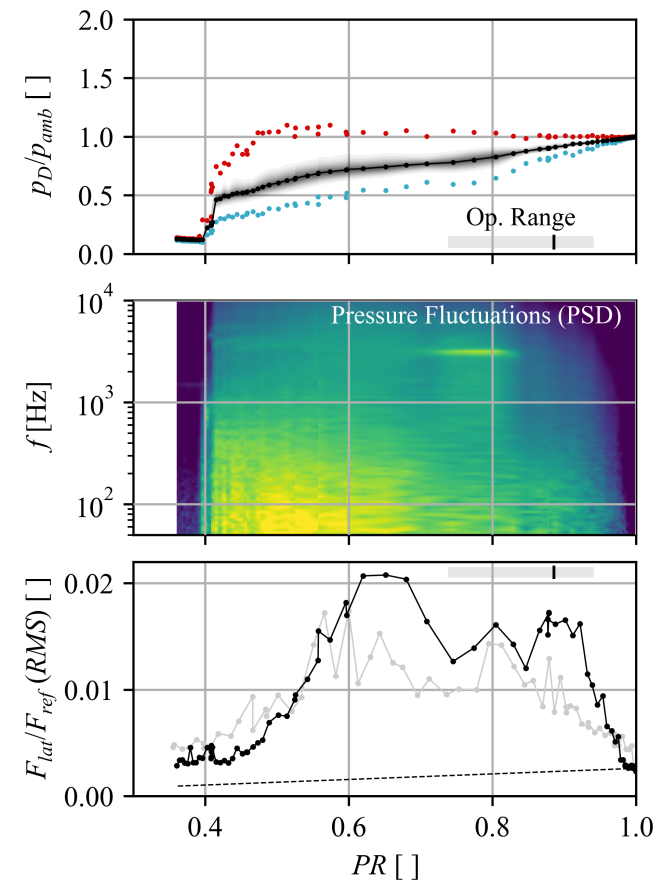
(c) *OR* = 0.10 ⌒

Figure A5. Wall pressure trends, frequency spectra, and dynamic load for the Concave geometry.

Int. J. Turbomach. Propuls. Power **2023**, *8*, 55

17 of 17

References

1. Cziesla, F.; Hencke, E.G.; Kather, A.; Keller, D.; Rukes, B. Statusreport—Fossil befeuerte Großkraftwerke in Deutschland—Stand, Tendenzen, Schlussfolgerungen, December 2013. VDI. Available online: https://web.archive.org/web/20140730025014/http://m.vdi.de/uploads/media/3544_BRO_TW_GEU_Statusreport_Fossil_befeuerte_Grosskraftwerke.pdf (accessed on 15 September 2022).
2. European Commission Commission Regulation (EU) 2016/631 of 14 April 2016 establishing a network code on requirements for grid connection of generators. *Official Journal of the European Union* **2016**, *59*, L 112/1. Available online: https://eur-lex.europa.eu/eli/reg/2016/631/oj (accessed on 19 September 2023).
3. Ess, F.; Peter, F.; Klumpp, F. Agora Energiewende (2017): Flexibility in Thermal Power Plants—With a Focus on Existing Coal-Fired Power Plants. 6 June 2017 *115/04-S-2017/EN*. Available online: https://www.agora-energiewende.org/fileadmin/Projekte/2017/Flexibility_in_thermal_plants/115_flexibility-report-WEB.pdf (accessed on 19 September 2023).
4. Domnick, C.B.; Brillert, D. Flow-Induced Steam Valve Vibrations—A Literature Review of Excitation Mechanisms, Preventive Measures, and Design Improvements. *J. Eng. Gas Turbines Power* **2019**, *141*, 051009. [CrossRef]
5. Yonezawa, K.; Ogi, K.; Takino, T.; Tsujimoto, Y.; Endo, T.; Tezuka, K.; Morita, R.; Inada, F. Experimental and Numerical Investigation of Flow Induced Vibration of Steam Control Valve. In Proceedings of the ASME 2010 7th International Symposium on Fluid-Structure Interactions, Flow-Sound Interactions, and Flow-Induced Vibration and Noise, Montreal, QC, Canada, 1–5 August 2010; pp. 575–583. [CrossRef]
6. Hardin, J.; Kushner, F.; Koester, S. Elimination Of Flow-Induced Instability From Steam Turbine Control Valves. In Proceedings of the Thirty-Second Turbomachinery Symposium, Houston, TX, USA, 8–11 September 2003; pp. 99–108. [CrossRef]
7. Zeß, J.-P.; Polklas, T.; Joos, F. Experimental Investigation of the Flow in a Control Valve of an Industrial Steam Turbine. In Proceedings of the ASME Turbo Expo 2016: Turbomachinery Technical Conference and Exposition, paper n. GT2016-57215, Seoul, South Korea, 13–17 June 2016. [CrossRef]
8. Wallat, S.; Domnick, C.B.; Musch, C.; Brillert, D. A Test Rig Concept to Study Fluid Structure Interactions in a Steam Turbine Valve. In Proceedings of the ASME Turbo Expo 2018: Turbomachinery Technical Conference and Exposition, paper n. GT2018-75094, Oslo, Norway, 11–15 June 2018. [CrossRef]
9. Slama, V.; Rudas, B.; Šimurda, D.; Hála, J. Pressure Loss Analysis and its Prediction in Typical Valve Designs for Steam Turbines. In Proceedings of ASME Turbo Expo 2023: Turbomachinery Technical Conference and Exposition, paper n. GT2023-101134, Boston, MA, USA, 26–30 June 2023. [CrossRef]
10. Domnick, C.B.; Benra, F.K.; Brillert, D.; Dohmen, H.J.; Musch, C. Improving the Design of Steam Turbine Inlet Valves by Numerical Methods for Enhanced Part Load Operation. In Proceedings of the 11th European Conference on Turbomachinery Fluid Dynamics & Thermodynamics, paper n. ETC2015-107, Madrid, Spain, 23–27 March 2015.
11. Windemuth, C.; Lange, M.; Mailach, R. Introduction of a Novel Test Rig for the Investigation of Fluid-Structure Interaction Effects in Steam Turbine Control Valves using an Elastic Model. In Proceedings of the 13th European Conference on Turbomachinery Fluid Dynamics & Thermodynamics, Lausanne, Switzerland, 8–12 April 2019. [CrossRef]
12. Zhang, D.; Engeda, A.; Hardin, J.R.; Aungier, R.H. Experimental Study of Steam Turbine Control Valves. *Proc. Inst. Mech. Eng. C-J. Mech. Eng. Sci.* **2004**, *218*, 493–507. [CrossRef]
13. Windemuth, C.; Lange, M.; Mailach, R. Investigation of Unsteady Pressure Fluctuations in a Simplified Steam Turbine Control Valve. *J. Eng. Gas Turbines Power* **2021**, *143*, 081017. [CrossRef]
14. Windemuth, C.; Lange, M.; Mailach, R. Comparison of Steam Turbine Control Valve Geometries and Their Dynamic Behaviour at Part Load. In Proceedings of the 15th European Conference on Turbomachinery Fluid Dynamics & Thermodynamics, paper n. ETC2023-138, Budapest, Hungary, 24–28 April 2023. Available online: https://www.euroturbo.eu/publications/conference-proceedings-repository/ (accessed on 23 July 2023)